scientific reports

Check for updates

OPEN

Variance-resistant PTB7 and axially-substituted silicon phthalocyanines as active materials for high-Voc organic photovoltaics

Mario C. Vebber[1], Nicole A. Rice[1], Jaclyn L. Brusso[2] & Benoît H. Lessard[1,3]✉

While the efficiency of organic photovoltaics (OPVs) has improved drastically in the past decade, such devices rely on exorbitantly expensive materials that are unfeasible for commercial applications. Moreover, examples of high voltage single-junction devices, which are necessary for several applications, particularly low-power electronics and rechargeable batteries, are lacking in literature. Alternatively, silicon phthalocyanines (R_2-SiPc) are inexpensive, industrially scalable organic semiconductors, having a minimal synthetic complexity (SC) index, and are capable of producing high voltages when used as acceptors in OPVs. In the present work, we have developed high voltage OPVs composed of poly({4,8-bis[(2-ethylhexyl)oxy]benzo[1,2-b:4,5-b′]dithiophene-2,6-diyl}{3-fluoro-2-[(2-ethylhexyl)carbonyl] thieno [3,4 b]thiophenediyl}) (PTB7) and an SiPc derivative ($(3BS)_2$-SiPc). While changes to the solvent system had a strong effect on performance, interestingly, the PTB7:$(3BS)_2$-SiPc active layer were robust to spin speed, annealing and components ratio. This invariance is a desirable characteristic for industrial production. All PTB7:$(3BS)_2$-SiPc devices produced high open circuit voltages between 1.0 and 1.07 V, while maintaining 80% of the overall efficiency, when compared to their fullerene-based counterpart.

Organic photovoltaics (OPVs) are a promising solar energy technology with the potential for low manufacturing cost and quick energy payback[1,2]. OPVs can be fabricated by solution-based techniques, such as spin-coating, blade-coating and a variety of printing techniques, facilitating their integration into continuous, high throughput processing, which is unachievable with traditional silicon technology[1,3–5]. In the past 5 years, single-junction OPVs with record power conversion efficiencies (PCE) of 15–19% have been reported[6–9], approaching commercial solar cell performances. However, these high efficiencies are achieved using expensive small molecules and polymers, the production of which is not scalable as they require complex multi-step synthesis and purification methods[10–14]. Most of these state-of-the-art OPVs often excel in high current densities (*Jsc*) and fill factor (FF), while providing middling open-circuit voltage (*Voc*), between 0.7 and 0.8 V[6–9,15].

High-voltage OPVs are of great interest for certain applications, particularly in rechargeable batteries and low-power electronics, which always require a minimum voltage to operate[16–18]. While high *Voc*s can be obtained by tandem cells or cells in series, this requires all cells to produce similar currents, which is virtually impossible to achieve in applications where lighting is inhomogeneous[16]. Some ternary BHJs with *Voc*s above 0.9 V have been reported[19,20], albeit relying on high-cost, non-scalable materials. It remains that the *Voc* of the majority of single-junction photovoltaics rarely surpasses 0.8 V, including silicon-based devices. Recently, a few research groups have used simple and low-cost small molecules as non-fullerene acceptors (NFAs) in OPVs, and achieved $Voc \geq 1.0$ V[12,21–24]. Such architectures may hold the key for commercial viability as they can be manufactured on an industrial scale, provided that the efficiency and stability of the devices is sufficiently high[21,25].

Axially substituted silicon phthalocyanines (R_2-SiPc) are ideal candidates for low-cost, high- *Voc* acceptor materials[24,26,27]. While metal phthalocyanine (MPc) have been investigated in organic electronic applications for more than 50 year, R_2-SiPcs are relatively understudied, having emerged in recent years[28] and successfully incorporated in multiple new application, including organic thin-film transistors (OTFTs)[29–34], organic light-emitting diodes (OLEDs)[26,35,36] and in OPVs[24,26,37–40]. The synthetic complexity (SC) index[41] of R_2-SiPcs have been

[1]Department of Chemical and Biological Engineering, University of Ottawa, 161 Louis Pasteur, Ottawa, ON K1N 6N5, Canada. [2]Department of Chemistry and Biomolecular Sciences, University of Ottawa, 150 Louis Pasteur, Ottawa, ON K1N 6N5, Canada. [3]School of Electrical Engineering and Computer Science, University of Ottawa, 800 King Edward, Ottawa, ON K1N 6N5, Canada. ✉email: benoit.lessard@uottawa.ca

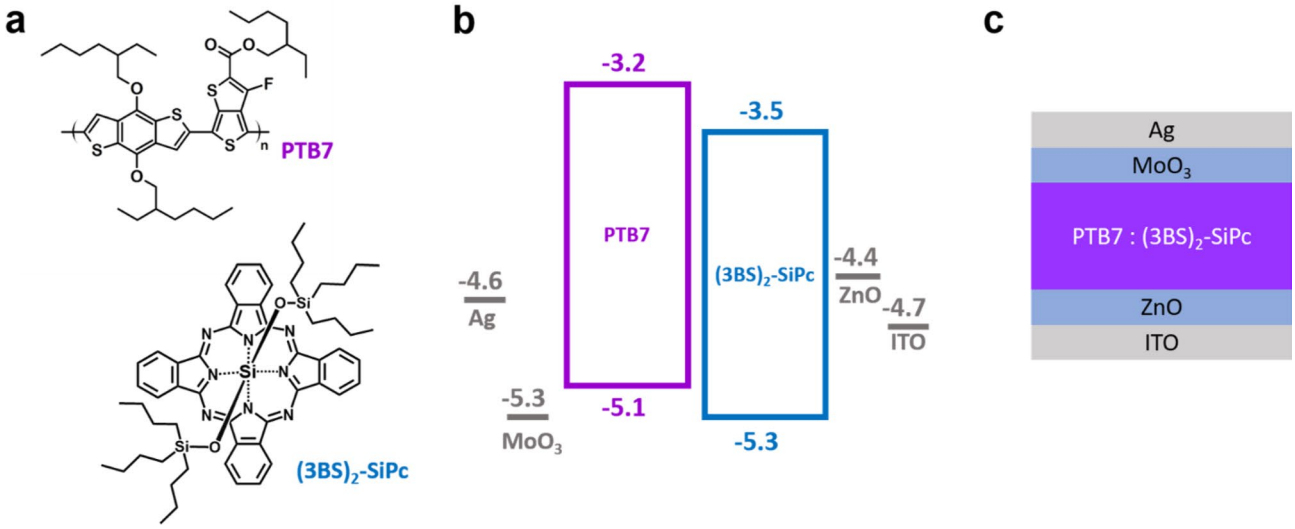

Figure 1. (**a**) Chemical structure of donor and acceptor materials; (**b**) energy level diagram of the device components; and (**c**) schematic representation of device architecture.

calculated to be at least three times lower (SC = 12)[27] than that of several prominent OPV acceptors materials, such as $PC_{61}BM$ (SC = 36)[42], Y6 (SC = 59)[43] and ITIC (SC = 67)[44]. The exceptionally low SC index of R_2-SiPcs makes them exceedingly promising organic semiconductors for OPVs. Historically, R_2-SiPcs have mainly been employed as ternary additives in OPVs[37–40,45]. However, in a recent study by Grant et al., an OPV composed of a blend of R_2-SiPc and poly-3-hexylthiophene (P3HT) achieved higher *Voc* and PCE than the fullerene-based analogue. Remarkably, when paired with poly[[4,8-bis[5-(2-ethylhexyl)-2-thienyl]benzo[1,2-b:4,5-b′]dithiophene-2,6-diyl]-2,5-thiophenediyl [5,7-bis(2-ethylhexyl)-4,8-dioxo-4H,8H-benzo[1,2-c:4,5-c′]dithiophene-1,3-diyl]] (PBDB-T), yielded a device with an exceptionally high *Voc* of nearly 1.1 V[24]. Additionally, relatively simple chemical modification of R_2-SiPcs can address other common issues in OPVs, such as stability, by including cross-linking groups in the SiPc structure to improve the stability of the active layer's nanostructure[46]. Nonetheless, there are relatively few reports investigating the use of R_2-SiPc as stand-alone acceptors in OPVs[24,26,27]. therefore it is vital to investigate pairing these cost-effective molecules with different donor polymers and optimizing these devices to exploit their full potential in OPVs.

In the present work we have fabricated OPVs using poly[[4,8-bis[(2-ethylhexyl)oxy]benzo[1,2-b:4,5-b']dithiophene-2,6-diyl][3-fluoro-2-[(2-ethylhexyl) carbonyl] thieno[3,4-b]thiophenediyl]] (PTB7, Fig. 1) and bis(tri-n-butylsilyl oxide) silicon phthalocyanine ($(3BS)_2$-SiPc; Fig. 1). Our group has recently reported similar devices, by pairing ($(3BS)_2$-SiPc with PBDB-T, and here we continue to explore this NFA with PTB7, another high performing polymer, that possesses more adequate energy level alignment with respect to ($(3BS)_2$-SiPc (Fig. 1). These devices were characterized by atomic force microscopy (AFM) and external quantum efficiency (EQE). The OPVs were optimized and yielded devices with a high *Voc* of 1.05 V, while maintaining 80% of the overall PCE, when compared to a fullerene-based analogue.

Experimental section

Materials. Two different molecular weights of PTB7 (93 kg mol^{-1}, PDI 2.6 and 16 kg mol^{-1}, PDI 2.4) was purchased from 1-Material and used as received. Bis(tri-n-butyl siloxy) silicon phthalocyanine ($(3BS)_2$-SiPc) was synthesized and purified according to the literature[45]. Dichlorobenzene (DCB, 99%), chlorobenzene (CB, 99%), chloroform (CF, 99%), dichloromethane (DCM, 99%), diiodooctane (DIO, 98%) and diphenylether (DPE, 99%), zinc acetate dehydrate ($Zn(Ac)_2 \cdot 2\,H_2O$, 99%), ethylamine (97%) were all purchased from Sigma-Aldrich and used without further purification. Ag (99.99%) was purchased from Angstrom Engineering Inc. and MoO_3 (99.99%) was purchased from Strem.

Devices. Indium-tin-oxide (ITO) coated glass substrates (100 nm, 20 Ω/sq, 1 in by 1 in), purchased from Thin Film Devices Inc., were cleaned in an ultrasound bath sequentially with soapy water, DI water, acetone (99%) and methanol (95%) to remove any debris. The ITO slides were then dried with a N_2 jet and placed in an air plasma cleaner for 15 min to remove any residual organics. The zinc oxide (ZnO) electron-transport layer was deposited by spin coating 150 µl of an ethanolic solution of $Zn(Ac)_2 \cdot 2\,H_2O$ (3.3%) and ethanolamine (0.9%) at 2000 RPM, followed by annealing for 1 h in air at 180 °C. The substrates were then move into a N_2 glovebox where the remainder of the procedure was carried out. Preparation of the active layer was achieved using a variety of conditions, details of which are provided in Table 1. The active layer components are illustrated in Fig. 1a. After deposition, the films were dried in the glovebox, at room temperature, for 1 h before being transferred to an evaporation chamber (Angstrom EvoVac), where MoO_3 (7 nm) and silver electrodes (70 nm) were deposited by physical vapor deposition at a pressure below 10^{-6} torr, to yield 5 individual 0.32 cm^2 devices per substrate, as defined by shadow masks. Energy level diagram and device architecture are shown in Fig. 1b and c,

#	D:A Ratio	Solvent	Spin speed: Annealing (RPM: °C/min)	Voc[a)] (V)	Jsc[a)] (mA cm^{-2})	FF[a)]	PCE[a)] (%)
1	1:1.5[b)]	CB	1500: N/A	0.76 ± 0.01	12.57 ± 0.3	0.49 ± 0.02	4.73 ± 0.03
2	1:1.5[b)]	CB + DIO (3%) + DPE (2%)	1500: N/A	0.70 ± 0.01	14.66 ± 0.09	0.65 ± 0.01	6.67 ± 0.09
3	1:1.5[c)]	CB	2000: N/A	1.05 ± 0.01	7.66 ± 0.08	0.45 ± 0.01	3.64 ± 0.05
4	1:1.5[c)]	CB	1500: N/A	1.06 ± 0.004	7.61 ± 0.04	0.45 ± 0.01	3.59 ± 0.01
5	1:1.5[c)]	CB	1000: N/A	1.06 ± 0.004	7.51 ± 0.05	0.43 ± 0.01	3.49 ± 0.01
6	1:1.5	CB	1500: 100/15	1.07 ± 0.01	7.58 ± 0.04	0.46 ± 0.01	3.55 ± 0.03
7	1:1.5	CB	1500: 100/30	1.00 ± 0.1	7.31 ± 0.05	0.47 ± 0.02	3.41 ± 0.2
8	1:1.5	CB	1500: 150/15	1.06 ± 0.01	7.11 ± 0.05	0.46 ± 0.02	3.48 ± 0.2
9	1:1.5	CB	1500: 150/30	1.03 ± 0.01	6.88 ± 0.09	0.44 ± 0.01	3.11 ± 0.08
10	1:1	CB	1500: N/A	1.06 ± 0.01	7.24 ± 0.04	0.44 ± 0.01	3.38 ± 0.02
11	1:1.5	CB	1500: N/A	1.05 ± 0.01	7.68 ± 0.2	0.46 ± 0.01	3.76 ± 0.1
12	1:1.8	CB	1500: N/A	1.05 ± 0.01	7.68 ± 0.07	0.48 ± 0.01	3.82 ± 0.04
13	1:2	CB	1500: N/A	1.04 ± 0.01	7.59 ± 0.03	0.48 ± 0.01	3.79 ± 0.03
14	1:1	DCB	1500: N/A	1.02 ± 0.004	7.48 ± 0.09	0.40 ± 0.01	3.06 ± 0.01
15	1:1.8	CB:CF 3:1	1500: N/A	1.04 ± 0.01	7.84 ± 0.09	0.45 ± 0.01	3.68 ± 0.04
16	1:1.8	CB:DCM 3:1	1500: N/A	1.06 ± 0.01	7.81 ± 0.05	0.45 ± 0.01	3.73 ± 0.01
17	1:1.8	CF	3000: N/A	1.02 ± 0.01	4.67 ± 0.1	0.38 ± 0.01	1.79 ± 0.08
18	1:1.5	CB + DIO (3%) + DPE (2%)	1500: N/A	No functioning device			
19	1:1.8[d)]	CB	1000: N/A	1.04 ± 0.004	5.84 ± 0.05	0.41 ± 0.01	2.47 ± 0.02
20	1:1.8[d)]	CB	1500: N/A	1.04 ± 0.004	6.19 ± 0.07	0.43 ± 0.01	2.74 ± 0.05

Table 1. Experimental conditions and resulting performance of PTB7:$(3BS)_2$-SiPc BHJ OPV devices. [a)]All BHJ OPVs were assessed under 1000 W m^{-2} light intensity, and scanned between − 2.0 and 2.0 V. The open circuit voltage (*Voc*), short circuit current (*Jsc*), fill factor (FF) and the power conversion efficiency (PCE) were obtained from an average of 4–8 devices with an individual area 0.32 cm^2 per device. Devices that have not been annealed are marked as "N/A". [b)]Baseline device composed of PTB7:$PC_{61}BM$ at a 1:1.5 ratio. [c)]Solution was not filtered before deposition. [d)]PTB7 with M_w of 96 kg mol^{-1} was used for all devices except device 19 and 20 where a M_w of 16 kg mol^{-1} was used.

respectively. Device performance was characterized using a custom push pin probe station connected to multiplexer and Keithley 2400 source meter. All OPVs were assessed under 1000 W m^{-2} light intensity, provided by a solar simulator (Xenon lamp, AM1.5) and scanned between − 2.0 and 2.0 V. Light intensity was verified using an NREL certified silicon standard cell prior to every run. Series and shunt resistances have been calculated from the slope of the IV curves, at the *Jsc* and *Voc*, respectively. External quantum efficiency (EQE) plots were recorded using a Newport Quantx-300 instrument outside of the glovebox. Prior to EQE measurements, the devices were encapsulated in an epoxy resin (Norland NOA61) cured under UV-light. Atomic force microscopy (AFM) topography images of the active layer films were obtained using a Bruker Dimension Icon instrument, with ScanAsyst-Air probes in tapping mode, at a frequency of 0.8 Hz; image processing was performed with NanoScope Analysis v1.8.

Results and discussion

Bulk heterojunction (BHJ) OPV devices (Fig. 1c) were fabricated by combining PTB7 (donor) with $(3BS)_2$-SiPc (acceptor, Fig. 1a). The energy levels of PTB7, $(3BS)_2$-SiPc and the other materials in the BHJ OPV devices are shown in Fig. 1b. Extensive optimization of the active layer was performed, as shown in Table 1. The optimized parameters were spin-rate, annealing, donor:acceptor ratio and choice of solvent. Parameters including spin-rate, annealing time and temperature, donor:acceptor ratio, and choice of solvent were all investigated.

The best PTB7:$(3BS)_2$-SiPc BHJ OPV device (**12**) was obtained with an excess of $(3BS)_2$-SiPc (1:1.8 ratio) in CB, at a spin rate of 1500 RPM, resulting in a high *Voc* of 1.05 ± 0.01 V, a modest J_{SC} of 7.68 ± 0.07 mA cm^{-2}, fill factor (*FF*) of 0.48 ± 0.01 and an overall PCE of 3.82 ± 0.04 (Table 1). While benchmark OPVs often have *FF* between 0.6 and 0.7[47], these values are comparable to those of the PTB7:$PC_{61}BM$ baseline device prepared (**1**). The average performance of device **12** is comparable to the champion device in the series, which achieved a PCE of 3.85% (*Voc* = 1.06 V, J_{SC} = 7.71 mA·cm^{-2}, FF = 0.47), within one standard deviation. These results are also slightly superior to the high-*Voc* devices previously reported by our group, based on PBDB-T/:$(3BS)_2$-SiPc devices (PCE = 3.4%)[24]. This improvement comes from a 10% improvement in current density, which can be attributed to the favourable energy level alignment between PTB7 and $(3BS)_2$-SiPc, with a 0.2–0.3 eV separation between HOMO and LUMO levels (Fig. 1). This energy gap facilitates charge separation and can lead to greater currents.

When optimizing the PTB7:$(3BS)_2$-SiPc BHJ OPV devices we found that PCE improves only slightly when deposition spin rate is increased from 1000 to 2000 RPM (devices **3**–**5**), demonstrating that the PTB7:$(3BS)_2$-SiPc active layer can be successfully deposited at different spin-rates. Interestingly, film thickness remains relatively constant, decreasing slightly from 129 to 115 nm, when varying spin rate from 1000 to 2000 RPM, which does

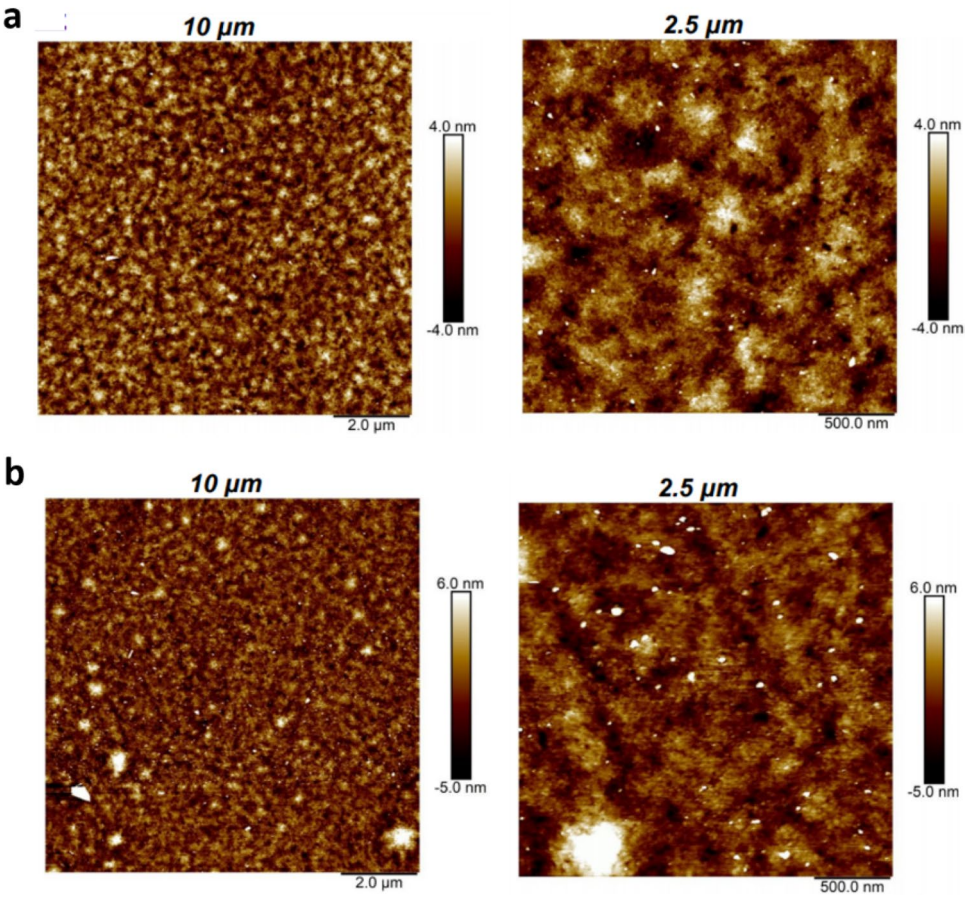

Figure 2. AFM height images of the PTB7:$(3BS)_2$-SiPc films on two different scales (10 and 2.5 μm (**a**) before annealing and (**b**) after annealing (15 min at 100 °C).

not follow the typical spin-coating equation, that predicts a thickness variation of nearly 50% between the two films[48]. This behaviour suggests a strong dilatant characteristic of the PTB7:$(3BS)_2$-SiPc solution, resisting the centrifugal force. While dilatant behaviour is common in polymer solutions, the extent of the effect observed here suggest strong interaction of PTB7 with the $(3BS)_2$-SiPc moieties in solution, leading to rheological modification. In general, annealing also showed a weak effect on device PCE (devices **6**–**9**), slightly increasing FF while decreasing *Jsc*. Figure 2 shows AFM images before (Fig. 2a) and after annealing for 15 min at 100 °C (Fig. 2b). Comparison of the films at various length scales shows that some larger amorphous features are formed during the annealing step, which is reflected in the increased roughness of the films: $r_q = 1.31$ nm before annealing and $r_q = 2.0$ nm after. Nonetheless, in general overall surface morphology and height features are mostly retained. Longer annealing times were slightly detrimental to device performance, most likely due to disruption of the active layer through formation of large agglomerates, as suggested in Fig. 2b. The $(3BS)_2$-SiPc to PTB7 ratio (devices **10**–**13**) only had a noticeable effect on the PCE when the ratio was reduced below 1.5, which is observed when comparing devices **10** and **11**, with ratios of 1.0 and 1.5, respectively. Alternatively, devices **11**, **12** and **13,** with ratios of 1.5, 1.8 and 2.0, respectively, have remarkably similar performances. While PTB7:PC_{61}BM devices have been optimized at a 1:1.5 ratio[49], the PTB7:$(3BS)_2$-SiPc BHJ OPV devices had the best performance when using a 1:1.8 ratio (Table 1). In summary, we found that the $(3BS)_2$-SiPc:PTB7 blend is fairly invariant to spin rate, acceptor:donor ratio and annealing conditions. This low variability is a desirable property for high throughput manufacture, where minor variations are inevitable.

Alternatively, modification of the active layer solvent system had a significant impact on device performance. Solvent additives, namely DIO and DPE, have been previously reported to play a critical role in the film morphology of the active layer in PTB7:PC_{61}BM devices, resulting in significant improvements in current density and PCE[50]. Such high boiling point additives promote higher crystallinity and improved nanomorphology in PTB7:fullerene blends[50], typically resulting in increases of more than 40% in PCE. We have observed these improvements as well in our baseline PTB7:PC_{61}BM baselines (**1** and **2,** Table 1). However, when incorporating these additives in the fabrication of PTB7:$(3BS)_2$-SiPc BHJ OPV devices (device **18**), we were unable to obtain functioning devices. This may be attributed to $(3BS)_2$-SiPc, which has been reported to crystallize rapidly[46,51,52], and the use of high boiling point additives thereby exacerbating this behaviour, creating micrometric or even submillimetric domains (patterns are visible to the naked eye) as opposed to the nanometric phase separation required for functioning OPVs[53,54]. In attempt to counter this crystallization we explored the use of low-boiling

Device	Series (Ω)	Shunt (Ω)	Thickness (nm)
P3HT:$PC_{61}BM$[45a)]	11	1676	200
P3HT:$(3BS)_2$-SiPc[24a)]	15	816	100
PTB7:$PC_{61}BM$ (**1**)	9	1352	90
PTB7:$(3BS)_2$-SiPc (**12**)	22	463	115

Table 2. Thickness, series and shunt resistances of the optimized devices and relevant comparative devices. [a)]Devices have been previously reported and further characterized here.

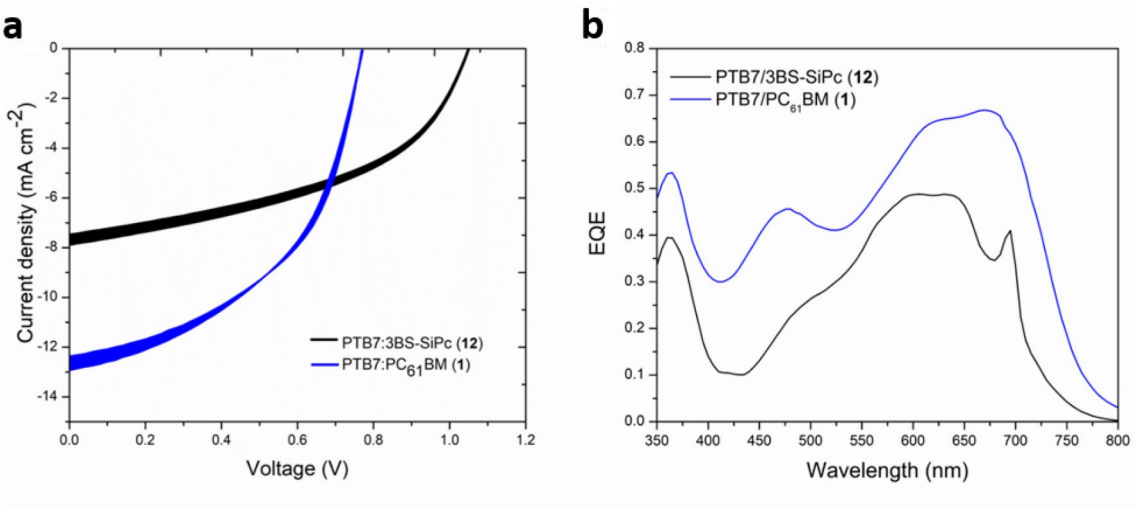

Figure 3. OPV characteristics (**a**) I–V curves, where line thickness corresponds to the standard deviation of 4 devices, and (**b**) EQE spectra of the optimized device (**12**) and the fullerene-containing baseline (**1**).

point solvent additives, such as DCM and CF (devices **15** and **16**) but these solvent changes led to negligible improvements in performance. Using CF as a single low-boiling point solvent (device **17**) resulted in thicker films due to rapid evaporation, which approximately halved the PCE when compared to the best devices deposited with solutions in CB. We have also investigated if incorporating a low a low-M_w PTB7 (16 kg mol^{-1}) instead of the conventional PTB7 (M_w = 96 kg mol^{-1}) could improve the crystallinity of the P7B7 phase without additives. Functioning devices were obtained (**19** and **20**), but with lower efficiency compared to the optimized device achieved from low-M_w PTB7 (**12**).

While the *Jsc* and FF of the PTB7:$(3BS)_2$-SiPc BHJ OPV devices were modest, it is important to note the consistently high *Voc* between 1.00 and 1.07 V, which is a very desirable and often rare characteristic in OPVs. Note that current state-of-the-art OPVs typically display *Voc* values around 0.8V[7–9]. The high voltages can be attributed to the large difference between the energy levels of the donor's highest occupied molecular orbital (HOMO) and the acceptor's lowest unoccupied molecular orbital (LUMO), as illustrated in Fig. 1b.

Table 2 compares the series and shunt resistances of our optimized device **12** with literature-based devices containing either PTB7 or P3HT as the donor and $PC_{61}BM$ or $(3BS)_2$-SiPc as the acceptor. Strikingly, the shunt resistance of the PTB7:$(3BS)_2$-SiPc BHJ OPV device is significantly lower than the others, which indicates a high rate of charge recombination in the active layer film[1,47] and may offer a potential explanation for the relatively low *Jsc* compared to PTB7:$PC_{61}BM$ devices (Table 1, 2). This may be ascribed to the small energy level offset only 0.2–0.3 eV between the donor and acceptor, which could be impairing the dissociation of excitons at the PTB7:$(3BS)_2$-SiPc interface[1]. Moreover, AFM images (Fig. 2) show that domain sizes are in the hundreds of nm range, which is often too large for optimal BHJ OPV operation, given the average distance travelled by excitons before recombination is around 5–15 nm[1,54,55].

Figure 3a shows the I–V curves for the optimized PTB7:$(3BS)_2$-SiPc device (**12**) compared to the PTB7:$PC_{61}BM$ baseline (**1**) and Fig. 3b displays the EQE curves for the same devices. While $(3BS)_2$-SiPc provides some extra light absorption around 700 nm, the overall quantum efficiency is lower than that of the fullerene-based device. This trade off is often seen in SiPc-based devices[24]. Both devices had similar shelf-life, retaining approximately 92% of their initial PCE after being stored for 6 months in N_2. Moreover, the EQE spectrum of device **12** is slightly blue-shifted and sharper in comparison to the baseline (**1**), which is associated with smaller crystallinity of the polymeric phase[50,56]. This suggests that $(3BS)_2$-SiPc inhibits the crystallization of PTB7, and it is one of the causes for the lower current observed when compared to the fullerene baseline. The lower crystallinity of the polymeric network can also impair charge conduction and contribute to the low shunt resistance measured for such devices. We surmise that a new type of additive, that simultaneously promotes the crystallization

of PTB7 while keeping the SiPc domain size small, could push the efficiency of this class of devices beyond that of the PTB7:$PC_{61}BM$ baseline, but the authors are not familiar with any additive that fits these requirements.

R_2-SiPcs continue to show promise as NFAs in BHJ OPVs. However, their tendency to quickly crystallize and their shallow LUMO level have been detrimental to achieving high performance. Moving forward, the chemical versatility of R_2-SiPc molecules, will facilitate fine tuning of the material properties such as their frontier orbital energy levels and the solid-state packing properties, providing the potential for improving device performance while still remaining synthetically simple molecules to produce.

Conclusion

We paired PTB7, a high performing donor polymer, with a low cost and easy to synthesize acceptor $(3BS)_2$-SiPc in OPVs and observed a significant improvement in *Voc* values. Device performance was robust to changes in the spin speed, acceptor:donor ratio and annealing; although this hinders a route towards device optimization, it is ultimately a desirable property for high throughput fabrication of OPVs. When replacing the fullerene acceptor with $(3BS)_2$-SiPc, 80% of the overall device efficiency was retained, while a high average *Voc* of 1.05 V was otained. These findings further establish SiPc-based acceptors as promising NFA candidates for high voltage OPV devices. Control of the crystallization of the SiPc will be key to yield the desired nanomorphology in the active layer will be key in the development of high performing device.

Received: 26 April 2021; Accepted: 15 July 2021
Published online: 28 July 2021

References

1. Fusella, M. A., Lin, Y. L. & Rand, B. P. *20—Organic Photovoltaics (OPVs): Device Physics* 2nd edn. (Elsevier Ltd, Amsterdam, 2019). https://doi.org/10.1016/B978-0-08-102284-9.00020-6.
2. Parida, B., Iniyan, S. & Goic, R. A Review of solar photovoltaic technologies. *Renew. Sustain. Energy Rev.* **15**(3), 1625–1636. https://doi.org/10.1016/j.rser.2010.11.032 (2011).
3. Cai, W., Gong, X. & Cao, Y. Polymer solar cells: recent development and possible routes for improvement in the performance. *Sol. Energy Mater. Sol. Cells* **94**(2), 114–127. https://doi.org/10.1016/j.solmat.2009.10.005 (2010).
4. You, J. *et al.* A polymer tandem solar cell with 10.6% power conversion efficiency. *Nat. Commun.* **4**, 1410–1446. https://doi.org/10.1038/ncomms2411 (2013).
5. Lipomi, D. J. Organic photovoltaics: focus on its strengths. *Joule* **2**(2), 195–198. https://doi.org/10.1016/j.joule.2017.12.011 (2018).
6. Yuan, J. *et al.* Single-junction organic solar cell with over 15 % efficiency using fused-ring acceptor with electron-deficient core single-junction organic solar cell with over 15 % efficiency using fused-ring acceptor with electron-deficient core. *Joule* **3**, 1–12. https://doi.org/10.1016/j.joule.2019.01.004 (2019).
7. Cui, Y. *et al.* Over 16% efficiency organic photovoltaic cells enabled by a chlorinated acceptor with increased open-circuit voltages. *Nat. Commun.* **10**(1), 1–8. https://doi.org/10.1038/s41467-019-10351-5 (2019).
8. Liu, Q. *et al.* 18% efficiency organic solar cells. *Sci. Bull.* **65**(4), 272–275. https://doi.org/10.1016/j.scib.2020.01.001 (2020).
9. Cui, Y. *et al.* Single-junction organic photovoltaic cells with approaching 18% efficiency. *Adv. Mater.* **32**(19), 1–7. https://doi.org/10.1002/adma.201908205 (2020).
10. Li, N. & Brabec, C. J. Air-processed polymer tandem solar cells with power conversion efficiency exceeding 10%. *Energy Environ. Sci.* **8**(10), 2902–2909. https://doi.org/10.1039/c5ee02145f (2015).
11. Zhao, J. *et al.* A difluorobenzoxadiazole building block for efficient polymer solar cells. *Adv. Mater.* **28**(9), 1868–1873. https://doi.org/10.1002/adma.201504611 (2016).
12 Hwang, Y. J., Li, H., Courtright, B. A. E., Subramaniyan, S. & Jenekhe, S. A. Nonfullerene polymer solar cells with 8.5% efficiency enabled by a new highly twisted electron acceptor dimer. *Adv. Mater.* **28**(1), 124–131. https://doi.org/10.1002/adma.201503801 (2016).
13. Zhang, J. *et al.* Conjugated polymer-small molecule alloy leads to high efficient ternary organic solar cells. *J. Am. Chem. Soc.* **137**(25), 8176–8183. https://doi.org/10.1021/jacs.5b03449 (2015).
14. Yang Michael, Y. *et al.* High-performance multiple-donor bulk heterojunction solar cells. *Nat. Photonics* **9**(3), 190–198. https://doi.org/10.1038/nphoton.2015.9 (2015).
15. Doumon, N. Y. *et al.* Energy level modulation of ITIC derivatives: effects on the photodegradation of conventional and inverted organic solar cells. *Org. Electron.* **69**, 255–262. https://doi.org/10.1016/j.orgel.2019.03.037 (2019).
16. Sullivan, P. *et al.* Ultra-high voltage multijunction organic solar cells for low-power electronic applications. *Adv. Energy Mater.* **3**(2), 239–244. https://doi.org/10.1002/aenm.201200560 (2013).
17. Sullivan, P. *et al.* Halogenated boron subphthalocyanines as light harvesting electron acceptors in organic photovoltaics. *Adv. Energy Mater.* **1**(3), 352–355. https://doi.org/10.1002/aenm.201100036 (2011).
18. Tipnis, R. *et al.* Large-area organic photovoltaic module-fabrication and performance. *Sol. Energy Mater. Sol. Cells* **93**(4), 442–446. https://doi.org/10.1016/j.solmat.2008.11.018 (2009).
19. Cheng, H. W. *et al.* Realizing efficient charge/energy transfer and charge extraction in fullerene-free organic photovoltaics via a versatile third component. *Nano Lett.* **19**(8), 5053–5061. https://doi.org/10.1021/acs.nanolett.9b01344 (2019).
20. Zhao, W., Li, S., Zhang, S., Liu, X. & Hou, J. Ternary polymer solar cells based on two acceptors and one donor for achieving 12.2% efficiency. *Adv. Mater.* https://doi.org/10.1002/adma.201604059 (2017).
21. Baran, D. *et al.* Reducing the efficiency-stability-cost gap of organic photovoltaics with highly efficient and stable small molecule acceptor ternary solar cells. *Nat. Mater.* **16**(3), 363–369. https://doi.org/10.1038/nmat4797 (2017).
22. Pascual-San-José, E. *et al.* Blade coated P3HT:non-fullerene acceptor solar cells: a high-throughput parameter study with a focus on up-scalability. *J. Mater. Chem. A* **7**(35), 20369–20382. https://doi.org/10.1039/c9ta07361b (2019).
23. Wadsworth, A. *et al.* Critical review of the molecular design progress in non-fullerene electron acceptors towards commercially viable organic solar cells. *Chem. Soc. Rev.* **48**(6), 1596–1625. https://doi.org/10.1039/c7cs00892a (2019).
24. Grant, T. M. *et al.* High voc solution-processed organic solar cells containing silicon phthalocyanine as a non-fullerene electron acceptor. *Org. Electron.* **87**, 105976. https://doi.org/10.1016/j.orgel.2020.105976 (2020).
25. Doumon, N. Y. *et al.* 1,8-diiodooctane acts as a photo-acid in organic solar cells. *Sci. Rep.* **9**(1), 1–14. https://doi.org/10.1038/s41598-019-40948-1 (2019).
26. Zysman-Colman, E. *et al.* Solution-processable silicon phthalocyanines in electroluminescent and photovoltaic devices. *ACS Appl. Mater. Interfaces* **8**(14), 9247–9253. https://doi.org/10.1021/acsami.5b12408 (2016).
27. Grant, T. M., Dindault, C., Rice, N. A., Swaraj, S. & Lessard, B. H. Synthetically facile organic solar cells with > 4% efficiency using P3HT and a silicon phthalocyanine non-fullerene acceptor. *Mater. Adv.* https://doi.org/10.1039/D1MA00165E (2021).

28. Mitra, K. & Hartman, M. C. T. Silicon phthalocyanines: synthesis and resurgent applications. *Org. Biomol. Chem.* https://doi.org/10.1039/d0ob02299c (2021).
29. Melville, O. A., Lessard, B. H. & Bender, T. P. Phthalocyanine-based organic thin-film transistors: a review of recent advances. *ACS Appl. Mater. Interfaces* **7**(24), 13105–13118. https://doi.org/10.1021/acsami.5b01718 (2015).
30. Melville, O. A. *et al.* Ambipolarity and air stability of silicon phthalocyanine organic thin-film transistors. *Adv. Electron. Mater.* **5**(1900087), 1–7. https://doi.org/10.1002/aelm.201900087 (2019).
31. Melville, O. A., Grant, T. M. & Lessard, B. H. Silicon phthalocyanines as N-type semiconductors in organic thin film transistors. *J. Mater. Chem. C* **6**(20), 5482–5488. https://doi.org/10.1039/c8tc01116h (2018).
32. Yutronkie, N. J., Grant, T. M., Melville, O. A., Lessard, B. H. & Brusso, J. L. Old Molecule, New chemistry: exploring silicon phthalocyanines as emerging N-type materials in organic electronics. *Materials (Basel).* **12**(8), 5–10. https://doi.org/10.3390/ma12081334 (2019).
33. Grant, T. M., Rice, N. A., Muccioli, L., Castet, F. & Lessard, B. H. Solution-processable n-type tin phthalocyanines in organic thin film transistors and as ternary additives in organic photovoltaics. *ACS Appl. Electron. Mater.* **1**(4), 494–504. https://doi.org/10.1021/acsaelm.8b00113 (2019).
34. King, B. *et al.* Silicon phthalocyanines for N-type organic thin-film transistors: development of structure–property relationships. *ACS Appl. Electron. Mater.* https://doi.org/10.1021/acsaelm.0c00871 (2021).
35. Pearson, A. J. *et al.* Silicon phthalocyanines as dopant red emitters for efficient solution processed OLEDs. *J. Mater. Chem. C* **5**(48), 12688–12698. https://doi.org/10.1039/c7tc03946h (2017).
36. Plint, T., Lessard, B. H. & Bender, T. P. Assessing the potential of group 13 and 14 metal/metalloid phthalocyanines as hole transport layers in organic light emitting diodes. *J. Appl. Phys.* **119**(14), 1455021–1455029. https://doi.org/10.1063/1.4945377 (2016).
37. Honda, S., Ohkita, H., Benten, H. & Ito, S. Multi-colored dye sensitization of polymer/fullerene bulk heterojunction solar cells. *Chem. Commun.* **46**(35), 6596–6598. https://doi.org/10.1039/c0cc01787f (2010).
38. Ke, L. *et al.* Panchromatic ternary/quaternary polymer/fullerene BHJ solar cells based on novel silicon naphthalocyanine and silicon phthalocyanine dye sensitizers. *J. Mater. Chem. A* **5**(6), 2550–2562. https://doi.org/10.1039/C6TA08729A (2017).
39. Honda, S., Yokoya, S., Ohkita, H., Benten, H. & Ito, S. Light-harvesting mechanism in polymer/fullerene/dye ternary blends studied by transient absorption spectroscopy. *J. Phys. Chem. C* **115**(22), 11306–11317. https://doi.org/10.1021/jp201742v (2011).
40. Ke, L. *et al.* A series of pyrene-substituted silicon phthalocyanines as near-IR sensitizers in organic ternary solar cells. *Adv. Energy Mater.* **6**(7), 1502355. https://doi.org/10.1002/aenm.201502355 (2016).
41. Po, R., Bianchi, G., Carbonera, C. & Pellegrino, A. "all That Glisters Is Not Gold": an analysis of the synthetic complexity of efficient polymer donors for polymer solar cells. *Macromolecules* **48**(3), 453–461. https://doi.org/10.1021/ma501894w (2015).
42. Andersen, T. R. *et al.* Novel cost-effective acceptor: P3HT based organic solar cells exhibiting the highest ever reported industrial readiness factor. *Mater. Adv.* **1**(4), 658–665. https://doi.org/10.1039/d0ma00133c (2020).
43. Brabec, C. J. *et al.* Material strategies to accelerate OPV technology toward a GW technology. *Adv. Energy Mater.* **10**(43), 1–10. https://doi.org/10.1002/aenm.202001864 (2020).
44. Du, X. *et al.* Efficient polymer solar cells based on non-fullerene acceptors with potential device lifetime approaching 10 years. *Joule* **3**(1), 215–226. https://doi.org/10.1016/j.joule.2018.09.001 (2019).
45. Vebber, M. C., Grant, T. M., Brusso, J. L. & Lessard, B. H. Bis (tri-alkylsilyl oxide) silicon phthalocyanines: understanding the role of solubility on device performance as ternary additives in organic photovoltaics. *Langmuir* **36**, 2612–2621. https://doi.org/10.1021/acs.langmuir.9b03772 (2020).
46. Grant, T. M., Gorisse, T., Dautel, O., Wantz, G. & Lessard, B. H. Multifunctional ternary additive in bulk heterojunction OPV: increased device performance and stability. *J. Mater. Chem. A* **5**(4), 1581–1587. https://doi.org/10.1039/c6ta08593h (2017).
47. Mazzio, K. A. & Luscombe, C. K. The future of organic photovoltaics. *Chem. Soc. Rev.* **44**(1), 78–90. https://doi.org/10.1039/c4cs00227j (2015).
48 Mouhamad, Y., Mokarian-Tabari, P., Clarke, N., Jones, R. A. L. & Geoghegan, M. Dynamics of polymer film formation during spin coating. *J. Appl. Phys.* https://doi.org/10.1063/1.4896674 (2014).
49. Ebenhoch, B., Thomson, S. A. J., Genevičius, K., Juška, G. & Samuel, I. D. W. Charge carrier mobility of the organic photovoltaic materials PTB7 and PC71BM and its influence on device performance. *Org. Electron.* **22**, 62–68. https://doi.org/10.1016/j.orgel.2015.03.013 (2015).
50. Zheng, Y. *et al.* Binary solvent additives treatment boosts the efficiency of PTB7: PCBM polymer solar cells to over 9.5%. *Sol. RRL* **2**(4), 1–8. https://doi.org/10.1002/solr.201700144 (2018).
51. Lessard, B. H. *et al.* Bis(Tri- n -Hexylsilyl Oxide) silicon phthalocyanine: a unique additive in ternary bulk heterojunction organic photovoltaic devices. *ACS Appl. Mater. Interfaces* **6**(17), 15040–15051. https://doi.org/10.1021/am503038t (2014).
52. Dang, M.-T. *et al.* Bis(Tri-n-Alkylsilyl Oxide) silicon phthalocyanines: a start to establishing a structure property relationship as both ternary additives and non-fullerene electron acceptors in bulk heterojunction organic photovoltaic devices. *J. Mater. Chem. A* **126**, 3378–3379. https://doi.org/10.1039/C6TA10739G (2017).
53. Wodo, O., Tirthapura, S., Chaudhary, S. & Ganapathysubramanian, B. A graph-based formulation for computational characterization of bulk heterojunction morphology. *Org. Electron.* **13**(6), 1105–1113. https://doi.org/10.1016/j.orgel.2012.03.007 (2012).
54. Lyons, B. P., Clarke, N. & Groves, C. The Relative importance of domain size, domain purity and domain interfaces to the performance of bulk-heterojunction organic photovoltaics. *Energy Environ. Sci.* **5**(6), 7657–7663. https://doi.org/10.1039/c2ee21327c (2012).
55. Martín-Gomis, L. *et al.* Distance-dependent electron transfer kinetics in axially connected silicon phthalocyanine-fullerene conjugates. *ChemPhysChem* **21**(20), 2254–2262. https://doi.org/10.1002/cphc.202000578 (2020).
56. Grell, M. *et al.* Chain geometry, solution aggregation and enhanced dichroism in the liquid-crystalline conjugated polymer poly(9,9-dioctylfluorene). *Acta Polym.* **49**(8), 439–444. https://doi.org/10.1002/(SICI)1521-4044(199808)49:8%3c439::AID-APOL439%3e3.0.CO;2-A (1998).

Acknowledgements

The Natural Sciences and Engineering Research Council of Canada (NSERC) (2015-509 03987 and STPGP 506661-17 to B.H.L), the Canada Research Chairs Program 950-230724 (B.H.L.). We also thank the Centre for Research in Photonics at the University of Ottawa (CRPuO) for access to the AFM.

Author contributions

M.V. synthesized all materials , fabricated and characterized all devices, and wrote the first draft of the manuscript. N.A.R. performed all AFM analysis and edited manuscript. B.H.L. obtained funding, developed project and established research infrastructure necessary for project. J.L. B. and B.H.L co-supervised and mentored students as well as aided in manuscript editing.

Competing interests
The authors declare no competing interests.

Additional information
Correspondence and requests for materials should be addressed to B.H.L.

Reprints and permissions information is available at www.nature.com/reprints.

Publisher's note Springer Nature remains neutral with regard to jurisdictional claims in published maps and institutional affiliations.